

4

The Energy Balance of the Surface

4.1 CONTACT POINT

The surface of Earth is the boundary between the atmosphere and the land or ocean. Defining the location of this boundary can be difficult over a highly disturbed sea or over land surfaces with a variable plant canopy. We will assume that the location of the surface can be appropriately defined, and we will treat it as a simple interface between two media. However, in considering the important energy exchange processes we must include the atmosphere and oceanic boundary layers and the first few meters of soil. The energy fluxes across the surface are as important to the climate as the fluxes at the top of the atmosphere, especially because the climate at the surface is of most practical significance. The surface energy balance determines the amount of energy available to evaporate surface water and to raise or lower the temperature of the surface. Surface processes also play an important role in determining the overall energy balance of the planet.

The energy budget at the surface is more complex than the budget at the top of the atmosphere because it requires consideration of fluxes of energy by conduction and by convection of heat and moisture through fluid motion, as well as by radiation. The local surface energy budget depends on the insolation, the surface characteristics such as wetness, vegetative cover, albedo, and on the characteristics of the overlying atmosphere. The energy budget of the surface is intimately related to the hydrologic cycle, because evaporation from the surface is a key component in the budgets of both energy and water. Understanding the energy budget of the surface is a necessary part of understanding climate and its dependence on external constraints.

4.2 THE SURFACE ENERGY BUDGET

The energy budget can be written in terms of energy flux per unit area passing vertically through the air–surface interface and is measured in watts per square meter. The processes that determine energy transfer between the surface and atmosphere include solar and infrared radiative transfer, fluxes of energy associated with fluid motions of the atmosphere and ocean, and movement of energy through the soil. For the purposes of energy-budget computations, surface storage takes place in that volume between the boundary with the atmosphere and a depth below the surface where energy fluxes and the storage rate of energy are considered negligible. This depth can be as little as a few meters in dry land areas or as much as several kilometers in oceanic areas where deep water is formed. For water surfaces, the horizontal energy fluxes accomplished by the fluid motions under the surface can be very important. The surface energy balance can be written symbolically as (4.1),

$$\frac{\partial E_s}{\partial t} = G = R_s - LE - SH - \Delta F_{eo} \quad (4.1)$$

where $\partial E_s / \partial t = G$ is the storage of energy in the surface soil and water, R_s is the net radiative flux of energy into the surface, LE is the latent heat flux from the surface to the atmosphere, SH is the sensible heat flux from the surface to the atmosphere, and ΔF_{eo} is the horizontal flux out of the column of land–ocean below the surface.

Under steady-state conditions in which the storage of energy is small, such as one might assume to hold for annual averages or for daily averages over land, the energy balance is between radiative heating and the processes that remove energy from the surface.

$$R_s = LE + SH + \Delta F_{eo} \quad (4.2)$$

Under most conditions, radiation heats the surface and latent and sensible heat fluxes cool it, so that the radiative, latent, and sensible heat flux terms in (4.1) and (4.2) are most often positive (Fig. 4.1).

The physical meaning of (4.1) is that the storage of energy below the surface is equal to the net radiative input minus the heat lost from the surface by evaporation, sensible heat flux, and horizontal heat transport to other latitudes or longitudes. In constructing (4.1) we have left out a multitude of other terms that can be important locally or for brief periods. These terms include the following:

- The latent heat of fusion required for melting ice and snow in spring may require 10% of the radiative imbalance for limited periods.
- Conversion of the kinetic energy of winds and waves to thermal energy is generally small.

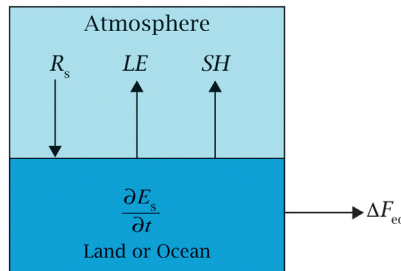


FIGURE 4.1 The relationship of the various terms in the surface energy balance. R_s , net radiation; LE, evaporative cooling; SH, sensible cooling; $\partial E_s / \partial t$, heat storage below the surface; ΔF_{eo} , divergence of horizontal energy flux below the surface.

- Heat transfer by precipitation can occur if the precipitation is at a different temperature than the surface. This mechanism is particularly important during summer showers, because the precipitation can be much cooler than the surface, and the thermal capacity of water is large.
- Some solar energy is not realized as heat, but is stored in the chemical bonds formed during photosynthesis. This is less than 1% globally, but can be $\sim 5\%$ locally for limited periods of time.
- Heat release by oxidation of biological substances, as in biological decay or forest fires, is the reverse of photosynthesis. Energy bound up in biological matter during photosynthesis is returned to the physical climate system through oxidation. This process takes place year round, but proceeds most rapidly when the surface is warm and moist.
- Geothermal energy release in hot springs, earthquakes, and volcanoes is small in a global sense.
- Heat released by fossil fuel burning or nuclear power generation can be important locally, but is not significant for the global energy balance.

4.3 STORAGE OF HEAT IN THE SURFACE

Energy storage in the surface is very important for the seasonal cycle of temperature over the oceans and the diurnal cycle over land and ocean. Using the simplest description, the amount of energy in the surface may be written as the product of an effective heat capacity for the earth–ocean system and a corresponding mean temperature,

$$E_s = \bar{C}_{co} T_{eo} \quad (4.3)$$

where \bar{C}_{eo} is the effective heat capacity of the land or ocean system ($J\ m^{-2}\ K^{-1}$) and T_{eo} is the effective temperature of the land or ocean energy-storing material (K).

The heat capacity depends on the physical properties of the surface materials and the depth of the surface layer that communicates with the atmosphere on the time scale of interest. It is generally only the first few meters of soil that respond to seasonal forcing of the surface energy balance, but the temperature of the top 50–100 m of ocean changes with the seasons. The depth of ocean that exchanges energy with the surface varies seasonally, so that possible time dependence of the effective heat capacity must be considered.

The heat capacity of the atmosphere is estimated by including only the energy associated with the motion of the molecules, which is related to the temperature. The heat capacity is the amount of energy that is required to raise the temperature by 1°. We may approximate the specific heat of air by the specific heat at constant pressure for dry air. To obtain the heat capacity for the entire atmosphere, we integrate over the mass of the atmosphere to get

$$\bar{C}_a = c_p \frac{p_s}{g} = \frac{1004\ J\ K^{-1}\ kg^{-1} \times 10^5\ Pa}{9.81\ ms^{-2}} = 1.02 \times 10^7\ J\ K^{-1}\ m^{-2} \quad (4.4)$$

One can estimate the thermal capacity of the ocean by using the thermal capacity of pure liquid water at 0°C. The thermal capacity for an arbitrary depth of water, d_w , can be obtained from the density ρ_w and the specific heat c_w ,

$$\begin{aligned} \bar{C}_o &= \rho_w c_w d_w = 10^3\ kg\ m^{-3} \times 4218\ J\ K^{-1}\ kg^{-1} \times d_w \\ &= d_w \times 4.2 \times 10^6\ J\ K^{-1}\ m^{-2}\ m^{-1} \end{aligned} \quad (4.5)$$

Comparing (4.4) and (4.5) we see that the thermal capacity of the atmosphere is equal to that of a little over 2 m of water. As discussed in Chapter 7, about the top 70 m of ocean interact with the atmosphere on the time scale of a year, so that on the seasonal time scale the thermal capacity of the ocean is about 30 times that of the atmosphere.

4.3.1 Heat Storage in Soil

The land has a much smaller effective heat capacity than the ocean. Because the surface is solid, it does not have the efficient heat transport by fluid motions that occurs in the atmosphere and ocean. Heat is transferred through the soil mostly by the less efficient process of conduction. Only the top 1 or 2 m of the soil is affected by seasonal variations.

TABLE 4.1 Properties of Soil Components at 293 K

	Specific heat (c_p) (J kg ⁻¹ K ⁻¹)	Density (ρ) (kg m ⁻³)	ρc_p (J m ⁻³ K ⁻¹)
Soil inorganic material	733	2600	1.9×10^6
Soil organic material	1921	1300	2.5×10^6
Water	4182	1000	4.2×10^6
Air	1004	1.2	1.2×10^3

After Brutsaert, 1982. Reprinted with permission from Kluwer Academic Publishers.

The heat capacity of a land surface is typically slightly smaller than that of the atmosphere.

The vertical flux of energy by conduction in the soil is proportional to the vertical temperature gradient in the soil,

$$F_s = -K_T \frac{\partial T}{\partial z} \quad (4.6)$$

where K_T is the thermal conductivity. The heat balance in the soil is between storage in the soil and convergence of the diffusive heat flux.

$$C_s \frac{\partial T}{\partial t} = -\frac{\partial}{\partial z}(F_s) = \frac{\partial}{\partial z} \left(K_T \frac{\partial T}{\partial z} \right) \quad (4.7)$$

The volumetric heat capacity of the surface material C_s is the product of the specific heat of the soil c_s , and the soil density ρ_s . The heat capacity of the soil depends on the volume fractions of soil f_s , organic matter f_c , water f_w , air f_a , and the density and specific heat of each component of the surface material.

$$C_s = \rho_s c_s f_s + \rho_c c_c f_c + \rho_w c_w f_w + \rho c_p f_a \quad (4.8)$$

From **Table 4.1**, it can be seen that the heat capacity of the air in the soil is very small, so that when water replaces air in the open spaces in the soil the heat capacity greatly increases. Porosity is the volumetric fraction of the soil that can be occupied by air or water.

Thermal conductivity of soils depends on the material, the porosity, and the soil water content. The thermal conductivity increases with water content for soils with relatively high porosity. Values vary from $0.1 \text{ Wm}^{-1} \text{ K}^{-1}$ for dry peat to $2.5 \text{ Wm}^{-1} \text{ K}^{-1}$ for wet sand. Under the condition that the thermal conductivity, K_T , is independent of depth, (4.7) simplifies to the heat equation

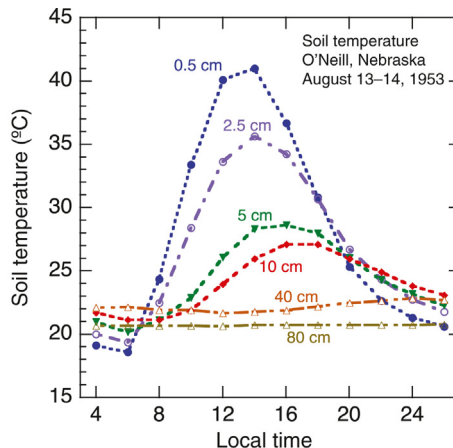


FIGURE 4.2 Soil temperature at various depths under a grass field at O'Neill, Nebraska on August 13, 1953. As a function of time of day. Measured thermal diffusivities on the day illustrated range from $2.5 \times 10^{-7} \text{ m}^2 \text{ s}^{-1}$ at 1 cm to $6 \times 10^{-7} \text{ m}^2 \text{ s}^{-1}$ at 5-cm depth in the soil. Data from Lettau and Davidson (1957).

$$\frac{\partial T}{\partial t} = D_T \frac{\partial^2 T}{\partial z^2} \quad (4.9)$$

where $D_T = K_T / C_s$ is the thermal diffusivity of the surface material. A simple scale analysis of (4.9) can be used to determine the depth through which a temperature anomaly applied at the surface will penetrate in a given time. One can show that the penetration depth, h_T , of temperature anomalies associated with a periodic forcing of temperature at the surface is given by

$$h_T = \sqrt{D_T \tau} \quad (4.10)$$

where τ is the time scale of the periodic forcing at the surface. Taking a typical value of soil diffusivity of $D_T = 5 \times 10^{-7} \text{ m}^2 \text{ s}^{-1}$, we obtain a penetration depth of about 10 cm for diurnal forcing and about 1.5 m for annual forcing. A surface temperature variation with a time scale of 10,000 years would penetrate the surface material to a depth of about 150 m. Because of the slow rates at which heat can be transported through soil and rock by conduction, horizontal heat transport under the land surface can be ignored in climate modeling.

Figure 4.2 shows temperatures at various depths in the soil as a function of time during a clear day in summer. The near surface soil experiences a large diurnal variation in temperature with minimum temperatures just before sunrise and maximum temperatures shortly after noon. Deeper

in the soil, the temperature variations are smaller and occur later in the day because of the time it takes the temperature pulse to diffuse into the soil. The amplitude of the temperature perturbation decreases to about e^{-1} of its surface value at about 10 cm below the surface and is very small by 40 cm below the surface. This observed decrease in the amplitude of the diurnal temperature perturbation is consistent with the simple dimensional arguments given previously.

The temperature data can be used to infer the thermal conductivity as a function of depth in the soil through the use of (4.7). Alternatively, if the vertical profiles of C_s and K_T are known and assumed constant with time, then measured temperature profiles in a deep layer of Earth can be used to estimate past variations in surface temperature on time scales of hundreds to thousands of years (Huang et al., 2000).

4.4 RADIATIVE HEATING OF THE SURFACE

The net input of radiative energy to the surface is the sum of the net solar and longwave flux densities at the surface,

$$R_s = S^\downarrow(0) - S^\uparrow(0) + F^\downarrow(0) - F^\uparrow(0) \quad (4.11)$$

where $S^\downarrow(0)$ and $S^\uparrow(0)$ are the downward and upward flux of solar radiation at the surface, respectively, and $F^\downarrow(0)$ and $F^\uparrow(0)$ represent similarly defined longwave fluxes.

4.4.1 Absorption of Solar Radiation at the Surface

The net downward solar energy flux can be written as the product of the downward solar flux at the surface multiplied by the absorptivity of the surface.

$$S^\downarrow(0) - S^\uparrow(0) = S^\downarrow(0)(1 - \alpha_s) \quad (4.12)$$

The surface albedo, α_s , is defined as the fraction of the downward solar flux density that is reflected by the surface.

The surface albedo varies widely depending on the surface type and condition, ranging from values as low as 5% for oceans under light winds to as much as 90% for fresh, dry snow. The numbers in Table 4.2 are characteristic, but each surface type can exhibit a range of albedos (Figs. 4.3 and 4.4). The most common surface is that of water, and its albedo depends on solar zenith angle, cloudiness, wind speed, and impurities in the water. The surface albedo of ocean under clear skies increases dramatically as the Sun approaches the horizon. Clouds scatter radiation very effectively, so that the solar radiation under a cloud is no longer a parallel beam but

TABLE 4.2 Albedos for Various Surfaces in Percent

Surface type	Range	Typical value
WATER		
Deep water: low wind, low altitude	5–10	7
Deep water: high wind, high altitude	10–20	12
BARE SURFACES		
Moist dark soil, high humus	5–15	10
Moist gray soil	10–20	15
Dry soil, desert	20–35	30
Wet sand	20–30	25
Dry light sand	30–40	35
Asphalt pavement	5–10	7
Concrete pavement	15–35	20
VEGETATION		
Short green vegetation	10–20	17
Dry vegetation	20–30	25
Coniferous forest	10–15	12
Deciduous forest	15–25	17
SNOW AND ICE		
Forest with surface snow cover	20–35	25
Sea ice, no snow cover	25–40	30
Old, melting snow	35–65	50
Dry, cold snow	60–75	70
Fresh, dry snow	70–90	80

is scattered in all directions. Under a cloud, the photons that reach the surface come from all possible directions with about equal probability, so that beneath a sufficiently thick cloud it is impossible to tell where in the sky the sun is located. Therefore, the surface albedo under overcast skies is insensitive to solar zenith angle. The amount of solar energy that reaches the surface under overcast skies is sensitive to solar zenith angle, however, since clouds are very effective reflectors of solar radiation and their albedo is somewhat sensitive to solar zenith angle (Fig. 3.13).

The reflectivities of various surfaces depend on the frequency of radiation (Fig. 4.5). Clouds and snow are most reflective for visible radiation,



FIGURE 4.3 NASA Natural Color Satellite Image of Southwestern Alaska on January 15, 2012. Fresh snow on land is very bright, while sea ice with tendrils in Bristol Bay is slightly darker. The ocean is very dark, except where clouds obscure the dark surface. *Image courtesy MODIS Rapid Response Team at NASA GSFC.*

and become less reflective at near-infrared wavelengths, where substantial absorption by water occurs. Green plants have a very low albedo for *photosynthetically active radiation*, where chlorophyll absorbs radiation efficiently. Radiation in the wavelength band from about 0.4–0.7 μm is effective for photosynthesis and growing plants absorb more than 90% of it. At about 0.7 μm the albedo of green plants increases sharply, so their albedo for near-infrared radiation can be as high as 50%. Since nearly half of the solar energy that reaches the surface is at wavelengths longer than 0.7 μm , this increase in albedo is significant for the energy budget of the surface. Plants need wavelengths shorter than 0.7 μm for photosynthesis, but the near-infrared energy absorption at wavelengths longer than 0.7 μm heats the leaves without any conversion of energy to plant tissue. The higher albedos at wavelengths longer than 0.7 μm thus help the leaves to stay cool. When green plants die and dry out, their chlorophyll content decreases and their albedo at visible wavelengths increases, as shown by the example of a field of straw.

The albedo of vegetated surfaces depends on the texture and physiological condition of the plant canopy. Leaf canopies with complex

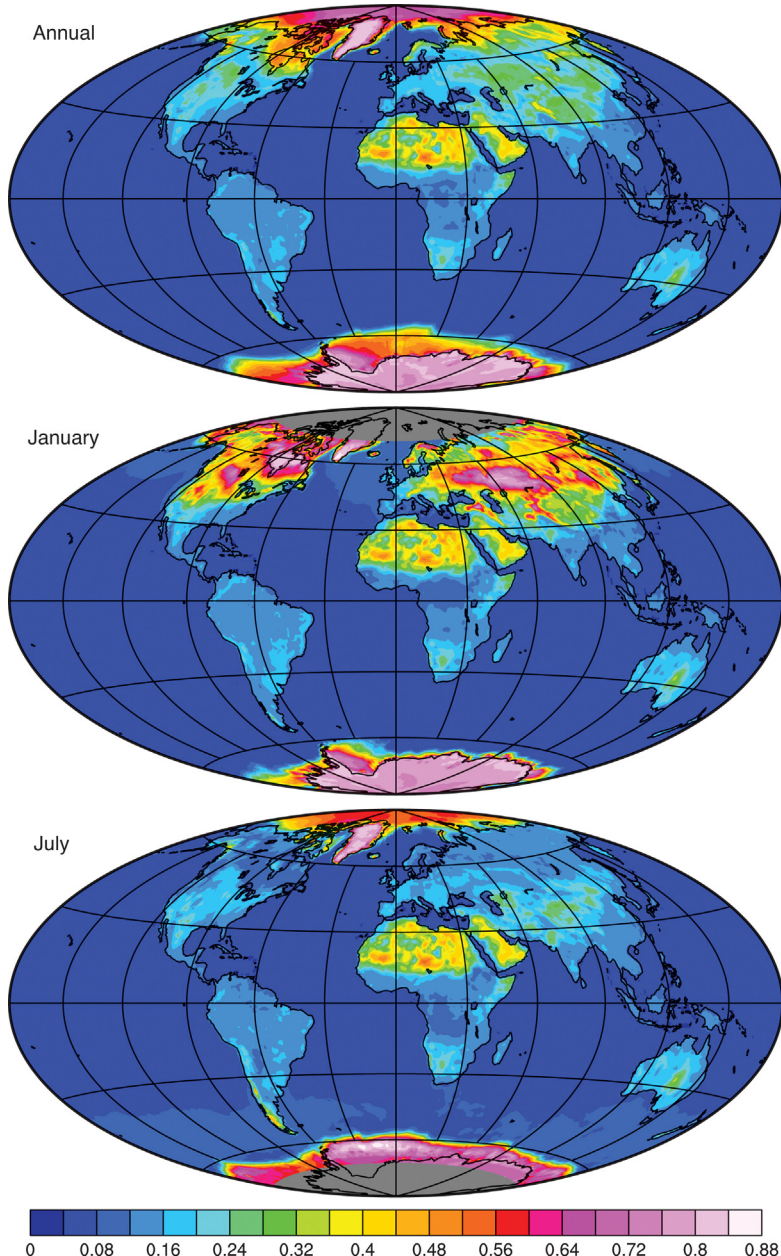


FIGURE 4.4 Surface albedo of Earth for annual mean, January and July. Gray areas indicate missing data. Data from NASA CERES surface albedo product.

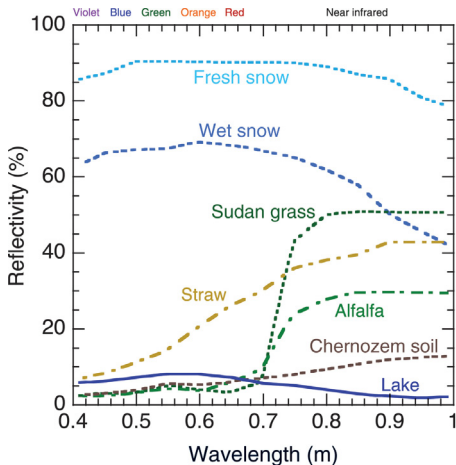


FIGURE 4.5 Surface reflectivity as a function of wavelength of radiation for a variety of natural surfaces. Human eyesight is sensitive to wavelengths from 0.4 μm (violet) to 0.7 μm (red). Alfalfa and sudan grass appear green because their albedo is higher for green light ($\sim 0.55 \mu\text{m}$) than for other visible wavelengths. Data from Mirinova (1973).

geometries and many cavities can have albedos that are lower than the albedo of an individual leaf. The ratio of near-infrared to visible radiation increases with depth below the top of the plant canopy, because the visible wavelengths are more effectively absorbed by leaves. The higher albedo of leaves for near-infrared radiation allows it to be scattered down through the plant canopy and heat the soil.

Pure water is most reflective for blue light. Natural water bodies contain many impurities and may be most reflective for green light, but their reflectance is generally higher at visible than at near-infrared wavelengths. Soils have higher reflectivities at near-infrared wavelengths than at visible wavelengths. Soils have significantly higher albedos when they are dry than when they are wet, and smooth soil surfaces have higher albedos than rough surfaces (Table 4.3).

Because surface albedo is highly variable and has a strong effect on absorbed solar radiation, it can have a large effect on surface temperature. Surface albedo can also have a strong effect on the sensitivity of climate, if it changes systematically with climatic conditions. Feedback processes involving surface albedo are discussed in Chapter 10.

4.4.2 Net Longwave Heating of the Surface

To calculate the net downward longwave radiation at the surface, one must know the downward longwave radiation coming from the atmosphere, the temperature of the surface, and the longwave emissivity of the surface, ε . If the frequencies of downward longwave radiation and

TABLE 4.3 Albedos for Dry and Moist Soil Surfaces

	Even surface		Tilled surface	
	Dry	Moist	Dry	Moist
Chernozem of dark gray color	13	8	8	4
Light chestnut soil of gray color	18	10	14	6
Chestnut soil of grayish red color	20	12	15	7
Gray sandy soil	25	18	20	11
White sand	40	20	—	—
Dark blue clay	23	16	—	—

From Mirinova, 1973.

radiation emitted from the surface are essentially the same, then the effective absorptivity of the surface is equal to its emissivity. Since this is approximately true, a fraction ε of the downward longwave radiation at the ground is absorbed, so that the upward longwave at the surface can be written

$$F^\uparrow(0) = (1 - \varepsilon) F^\downarrow(0) + \varepsilon \sigma T_s^4 \quad (4.13)$$

We may thus write

$$F^\downarrow(0) - F^\uparrow(0) = \varepsilon(F^\downarrow(0) - \sigma T_s^4) \quad (4.14)$$

Emissivities of some natural surfaces are given in **Table 4.4**. Most surfaces have very high emissivities. The great exceptions to this are polished metals, which have very low emissivities, so that metal films on plastic are very useful as emergency blankets or thermal shrouds for satellites, and

TABLE 4.4 Typical Thermal Infrared Emissivity for Selected Surfaces

Water	0.99	Glass, smooth uncoated	0.91
Ice and snow	0.98	Paper	0.87
Bare soil	0.96	Brick	0.90
Vegetation	0.96	Carbon	0.85
Stone pavement	0.96	Plastic	0.95
Wood	0.94	Mercury liquid	0.10
Asphalt, black	0.97	Silver, polished	0.02
Concrete	0.91	Gold, polished	0.02

Values vary based on the condition of the surface and wavelength.

metal films can also be used to make low emissivity glass for house windows that transmits visible light very well. Because of the strong greenhouse effect at work in Earth's atmosphere, the downward longwave from the atmosphere and the emission from the surface are both relatively large and tend to offset each other. The longwave emissivities of most natural surfaces are more than 0.95 and so variations of emissivity do not play a key role in the determination of surface climate. Inaccuracy in the estimation of surface emissivity can cause errors in the calculation of net longwave flux at the surface of about 5%. The errors in estimates of the surface temperature in equilibrium are much smaller, however, because in deriving the temperature from the energy flux balance, a one-fourth root is taken. This reduces the variation in surface temperature associated with emissivity variations to about 1%.

4.5 THE ATMOSPHERIC BOUNDARY LAYER

The *atmospheric boundary layer* is the lowest part of the troposphere, where the wind, temperatures, and humidity are strongly influenced by the surface. The wind speed decreases from its value in the free atmosphere to near zero at the surface. Fluxes of momentum, heat, and moisture by small-scale turbulent motions in the boundary layer communicate the presence of the lower boundary to the atmosphere and are critical to the climate. Aerosols and gaseous chemical constituents of the atmosphere are also exchanged with the surface through the atmospheric boundary layer. A characteristic of the atmospheric boundary layer is its quick response to changes in surface conditions. The response of the surface to the daily variation of insolation is felt strongly throughout the boundary layer, but in the free troposphere diurnal changes are usually small, unless thermal convection associated with daytime heating of the land surface penetrates deep into the atmosphere. Another important aspect of the boundary layer is the cloud that it contains. The most common type of cloud is marine boundary-layer cloud over the ocean, and this type of cloud appears to be both the most important in the energy balance of Earth and also probably the most important type of cloud in determining the sensitivity of climate change.

The depth of the atmospheric boundary layer can vary between about 20 m and several kilometers, depending on the conditions, but a typical boundary-layer depth is about 1 km. The boundary layer is generally deeper when the surface is being heated, when the winds are strong, when the surface is rough, and when the mean vertical motion in the free troposphere is upward.

Transports of mass, momentum, and energy through the boundary layer are accomplished by turbulent motions. If it were not for the

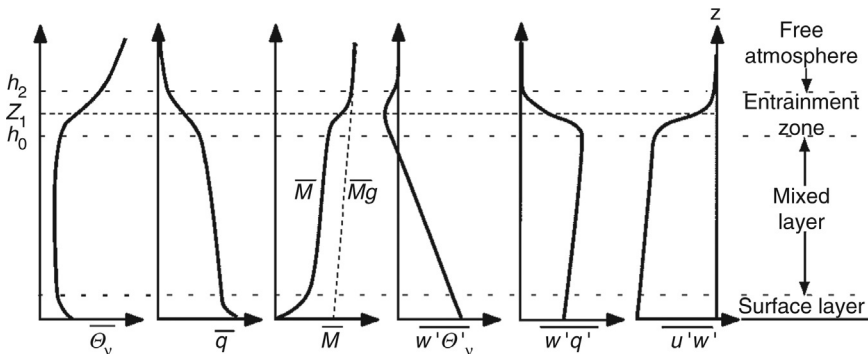


FIGURE 4.6 Structure of a convective boundary layer. It shows the distributions of mean virtual potential temperature $\bar{\Theta}_v$, water vapor mixing ratio \bar{q} , momentum \bar{M} , geostrophic momentum \bar{M}_g , and the vertical eddy fluxes of potential temperature, humidity, and momentum. From Stull (1988) after Dreidenks and Tennekes (1984). Reprinted with permission from Kluwer Academic Publishers.

chaotic swirls of turbulent motion in the boundary layer, the nonradiative exchange between the surface and the atmosphere would be extremely slow. The turbulent motions that carry the vertical fluxes in the boundary layer range in scale from the depth of the boundary layer to the smallest scales where molecular diffusion becomes an important transport mechanism. Turbulence can be generated thermally or mechanically. *Mechanical turbulence* is generated by the conversion of the mean winds to turbulent motions, and is strongest when the mean wind in the lower atmosphere is large. *Convective turbulence* is generated when warm air parcels near the surface are accelerated upward by their buoyancy. Convective turbulence is most easily observed over land surfaces during daylight hours, when strong solar heating of the surface provides a source of buoyant energy, but is also very common over the oceans. When the boundary layer is relatively unstable, so that buoyancy forces or shearing instabilities generate turbulence, the boundary layer may contain a well-mixed layer, where momentum, heat, and moisture are almost independent of height.

The structure of the planetary boundary layer varies widely, depending on the meteorological conditions and whether the surface is being heated or cooled. When a surface heat source is present, such as over land during the daytime, the boundary layer is often unstable and has a structure that is generally like that shown in Fig. 4.6. The lowest part of the boundary layer is called the *surface layer*, where the vertical fluxes of momentum, heat, and moisture are almost constant with height. In the mixed layer, buoyancy drives turbulent motions that maintain the potential temperature, $\bar{\Theta}_v$, the humidity, \bar{q} , and the momentum, \bar{M} , at values that are almost independent of height. Heat and moisture are transported upward in the mixed layer and momentum is transported downward toward the

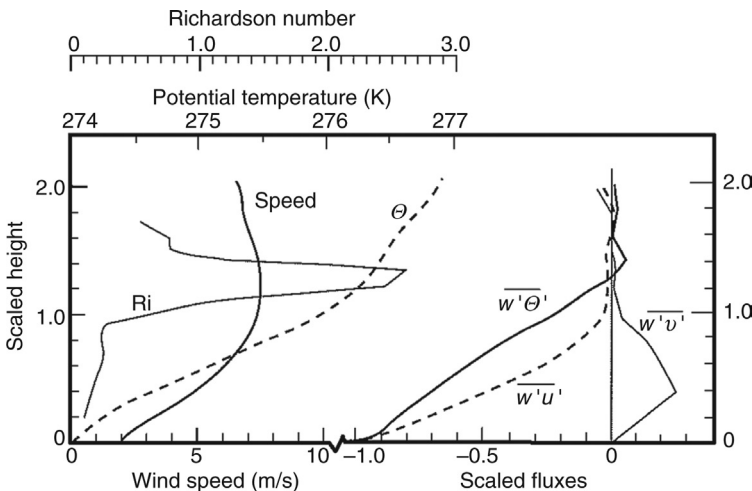


FIGURE 4.7 Averaged profiles of wind speed, potential temperature, Richardson number and vertical fluxes of potential temperature ($w'\bar{\theta}'$), and horizontal momentum ($w'u'$) and ($w'v'$) from nocturnal observations at Haswell, Colorado, on March 24, 1974. The height is scaled by the depth in which turbulence is observed to occur, which on average is about 100 m in this case. Vertical eddy fluxes are scaled by their surface values. *From Mahrt et al. (1979). Reprinted with permission from Kluwer Academic Publishers.*

surface. The top of the boundary layer is a transition zone between the boundary layer and the free atmosphere, which is often called the *entrainment zone*. Across this transition, the air properties change rapidly from those of the mixed layer to those of the free atmosphere above, generally marked by a decrease in humidity, an increase in potential temperature, and a decrease in the magnitude of the vertical fluxes of heat, moisture, and momentum by turbulent motions. *Entrainment* is the process whereby air from the free atmosphere is incorporated into the boundary layer. Entrainment is measured by a small downward eddy potential temperature flux in the entrainment zone. Entrainment adds mass to the boundary layer and is necessary when the boundary layer is deepening, or when the large-scale flow is downward into the boundary layer.

At night, longwave emission cools the land surface more rapidly than the air above it and the boundary layer can become very stable, with cold, dense air trapped near the surface (Fig. 4.7). Under these conditions, turbulence and the vertical fluxes it produces can be greatly suppressed, and the surface becomes mechanically uncoupled from the free atmosphere, although radiative transports can still occur. The potential temperature increases rapidly with height near the surface, and the transport of potential temperature is downward, so that less dense air is being forced downward against buoyancy. The energy for mixing less dense air downward toward the surface is provided by the mean wind speed shear, which tends

to be quite strong under these conditions, often with a low-level wind maximum near the top of the boundary layer and weak winds near the surface. The minimum surface-air temperature achieved on a clear night is thus generally lower when the wind speed in the free atmosphere is weak and provides little energy for mixing warm air downward to the radiatively cooled surface. On cool nights with high boundary layer stability, farmers may try to prevent crops from freezing by using propellers to generate mechanical turbulence that will mix warm air downward toward the surface.

The atmospheric boundary layer can contain clouds that play an important role in boundary-layer physics and vertical transports. The release of latent heat in clouds can provide buoyancy to drive vertical motions in the boundary layer. Boundary-layer clouds that are important for climate include the fair weather cumulus clouds and stratocumulus clouds. Though less widespread, fog is also an important boundary-layer cloud. The boundary layer also interacts in important ways with deep convective clouds, since the high potential temperature air that drives deep convection is produced in the boundary layer. Except when fog is present, the tops of boundary-layer clouds generally occur near the top of the boundary layer and their bases are some distance above the surface, so that a cloud and a subcloud layer exist within the boundary layer. Stratocumulus clouds modify the boundary-layer physics both through their convective heat and moisture fluxes and through their radiative effects. Because stratocumulus cloud tops are relatively warm and emit longwave radiation efficiently, longwave cooling from cloud tops can be an important mechanism for generating buoyancy within the boundary layer, since it cools the air at the top of the boundary layer, which then tends to sink and be replaced by warmer parcels of air rising from below.

Figure 4.8 shows the diurnal variation of temperature in the lowest 1500 m of the atmosphere over Nebraska during a relatively clear summer day. At sunrise, the surface is colder than the air 1 km above the surface. This temperature inversion quickly disappears after sunrise, as insolation warms the surface and this heat is transferred to a shallow layer of air near the ground. Near the middle of the day, the surface reaches its maximum temperature and a lapse rate near the dry adiabatic value of 9.8 K m^{-1} is observed near the surface. At this time, buoyancy raises warm parcels of air near the surface, and turbulent convection efficiently moves sensible heat upward in the boundary layer. Even before sunset, the surface begins to cool in response to efficient upward transport of energy by turbulent motions. After sunset the surface cools rapidly, so that by 10 PM the surface temperature has reached its nighttime value, leaving a very sharp inversion near the ground.

When mean wind speeds are light to moderate, diurnal variations in the temperature profile will affect the exchange of heat, moisture, and

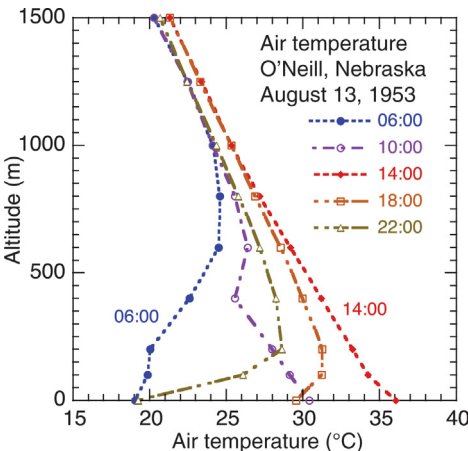


FIGURE 4.8 Plot of air temperature at various local times in the lowest 1500 m of the atmosphere at O'Neill, Nebraska on August 13, 1953. Times are given using a 24-h clock so that 1800 = 6 PM, etc. Data from Lettau and Davidson (1957).

momentum between the atmosphere and the surface. The strong density stratification associated with a nocturnal temperature inversion suppresses turbulent transport of momentum from the free atmosphere. Sensible and latent heat fluxes are also suppressed by the strong density stratification, so that the surface temperature responds primarily to the radiative forcing, which acts to cool the surface at night. Temperature inversions often develop when a high-pressure system dominates the local weather pattern. The weak surface winds, clear skies, and downward mean motion in the free atmosphere that are normally associated with high-pressure systems encourage the development of a strong inversion. Pollutants released under a temperature inversion can easily build up to unhealthy levels, because turbulent mixing into the free atmosphere is suppressed by the strong density gradient.

4.5.1 The Neutral Boundary Layer

When the static stability in the boundary layer is near neutral, buoyancy does not play an important role in the turbulent kinetic energy budget. Under neutral conditions, the source of energy for boundary-layer turbulence is the kinetic energy of the mean wind of the free atmosphere. The turbulence in the boundary layer produces a strong flux of momentum to the surface. The vertical flux of horizontal momentum at the surface, τ_0 , constitutes a drag on the atmospheric flow. In the surface layer, the vertical gradient of wind speed (U) under conditions of neutral stability should depend only on the height (z), density (ρ), and surface drag (τ_0).

The characteristic wind speed for use in dimensional analysis is the friction velocity, u_* .

$$u_* = \left(\frac{\tau_0}{\rho} \right)^{1/2} \quad (4.15)$$

Using the friction velocity and the height to scale the wind shear, dimensional analysis suggests that the scaled wind shear should be a constant.

$$\left(\frac{z}{u_*} \right) \frac{dU}{dz} = \frac{1}{\kappa} \quad (4.16)$$

The von Karman constant, κ , is the same for all neutral boundary layers regardless of the surface characteristics, and has a measured value of approximately 0.4. Equation (4.16) can be integrated with respect to height to obtain the logarithmic velocity profile.

$$U(z) = \left(\frac{u_*}{\kappa} \right) \ln \left(\frac{z}{z_0} \right) \quad (4.17)$$

An additional constant, z_0 , is introduced during the integration to obtain (4.17). It is called the *roughness height*, the height at which the wind speed reaches zero. For most natural surfaces the irregularities of the surface are larger than the 1 mm depth of the layer where molecular diffusion dominates, and this roughness can be characterized by the height z_0 . Roughness heights for natural surfaces range from about 1 mm for average seas to more than 1 m for cities with tall buildings. Roughness heights are estimated by measuring the wind-speed profile under neutral conditions and then solving (4.17) for z_0 . The logarithmic velocity profile has been shown to be a good approximation for many laboratory boundary layers and also for the planetary boundary layer under conditions of neutral stratification. It is valid for heights much greater than the roughness height, $z \gg z_0$, and so does not describe the mean wind-velocity profile within the plant canopy or very close to a rough surface.

The logarithmic velocity-profile law is useful for expressing the momentum flux at the surface in terms of the wind speed at some height in the surface layer. Substituting (4.15) into (4.17) yields an expression for the surface drag in terms of the wind speed, U_r , at some reference height z_r .

$$\tau_0 = \rho C_D U_r^2 \quad (4.18)$$

where

$$C_D = \kappa^2 \left\{ \ln \left(\frac{z_r}{z_0} \right) \right\}^{-2} \quad (4.19)$$

The drag coefficient, C_D , depends on the ratio of the reference height to the roughness height. The reference layer can be taken at any level within the surface layer where measurements can be conveniently acquired and where the logarithmic profile is a good approximation of the actual flow. The aerodynamic drag formula (4.18) and related formulas for the sensible and latent heat fluxes at the surface form the basis for empirical estimates of surface fluxes and the specification of surface fluxes in climate models. They allow the calculation of turbulent fluxes using only mean wind speed at a reference height and a few external parameters, and so are used in nearly all climate models and also for estimating surface turbulent fluxes from measurements of mean quantities.

4.5.2 Stratified Boundary Layers

The dimensional analysis for neutral boundary layers can be extended to stratified boundary layers (Monin and Obukhov, 1954; Arya, 1988). This theory adds heat flux and buoyancy variables to the dimensional analysis. Characteristic vertical profiles for both wind and temperature are derived in which the vertical coordinate is scaled by a dimensionless combination of the friction velocity, the heat flux, and the buoyancy. From these profiles, bulk aerodynamic formulas can be derived that describe the turbulent heat and momentum fluxes at the surface in terms of mean variables. The coefficients in these formulas now depend on the vertical stability of the atmosphere as well as the roughness height. This theory applies only to the surface layer.

The vertical stability can be characterized with the *Richardson number*. In differential form, the Richardson number depends on the vertical derivatives of potential temperature, Θ (see Chapter 1), and wind speed, U

$$Ri = \left(\frac{g}{T_0} \right) \frac{(\partial \Theta / \partial z)}{(\partial U / \partial z)^2} \quad (4.20)$$

where g is the gravitational acceleration and T_0 is the reference temperature. The bulk Richardson number for the boundary layer may be written as

$$Ri_B = \left(\frac{g}{T_0} \right) \left[\frac{z_r (\Theta(z_r) - \Theta(z_0))}{U(z_r)^2} \right] \quad (4.21)$$

The Richardson number indicates how likely the flow is to mix vertically in response to buoyancy and wind shear. The Richardson number is large when the potential temperature of the near surface air is high compared to the potential temperature at the surface. Under such conditions, the air is stably stratified, which inhibits vertical mixing. Parcels that are raised up from the surface become negatively buoyant and will be forced back downward by the gravity force. This stabilizing effect can be overcome by the kinetic energy available in the mean wind shear near the ground, which can generate turbulent velocities sufficient to mix stably stratified air. This influence of the kinetic energy is represented by the square of the wind speed in the denominator of (4.21). If the potential temperature decreases with height near the surface, then the boundary layer is unstable and the buoyancy force will accelerate small vertical displacements of parcels. The Richardson number for a buoyantly unstable boundary layer is negative. Under these conditions, vertical transfer of energy and moisture is relatively efficient because of the free exchange of parcels across level surfaces.

Over land areas, it is common for the boundary layer to become unstable during summer days as insolation heats the surface. At night, the surface cools faster than the overlying air so that a temperature inversion can develop (Fig. 4.8). The resulting strong-density stratification can suppress the nighttime exchanges of heat, momentum, and moisture between the surface and the free atmosphere. The effect of changes in the stability of the boundary layer on momentum fluxes can be seen in diurnal changes in the wind profile. Figure 4.9 shows the diurnal variations in wind speed

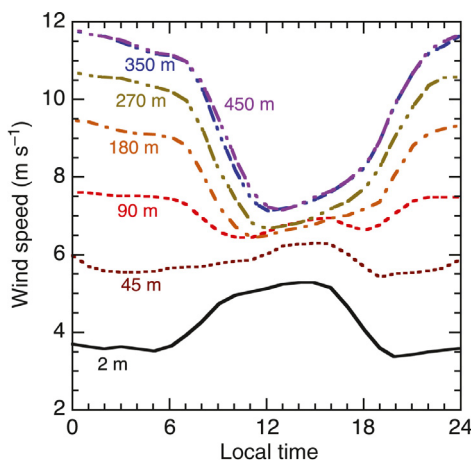


FIGURE 4.9 Diurnal cycle of wind speed as a function of height measured from a tower in Oklahoma City and averaged over the period from June 1966 to May 1967. Adapted from Crawford and Hudson (1973). Reprinted with permission from the American Meteorological Society.

measured at various heights on a TV tower in Oklahoma. At night, wind speeds measured very near the surface decrease, because the downward mixing of momentum from the free atmosphere is reduced by the greater static stability at night. The winds higher in the boundary layer increase at night because the drag from the surface is reduced. During the day, efficient mixing of momentum through a relatively unstable boundary layer causes the wind speed near the surface to increase at the expense of the wind speed higher in the boundary layer.

4.6 SENSIBLE AND LATENT HEAT FLUXES IN THE BOUNDARY LAYER

The turbulent fluid motions in the boundary layer produce sensible and latent heat fluxes from the surface. Transport by molecular diffusion is negligible compared to turbulent transport, except within about 1 mm of the surface. Turbulence is characterized by rapid chaotic fluctuations in wind velocity. Where mean vertical gradients in temperature or humidity exist, the turbulent fluctuations of wind velocity will be accompanied by fluctuations of scalar properties such as temperature and humidity. Vertical fluxes of mass, momentum, and energy are produced by turbulence when the parcels of air moving upward have different properties than parcels of air moving downward. Therefore, the flux can be measured by the spatial or temporal average of the product of vertical velocity and the property of interest.

For example, if we have measurements of the temperature, T , and vertical velocity, w , at a point near the surface, we may obtain the vertical flux of sensible heat from the time average of the product of vertical velocity and temperature, multiplied by the specific heat and average density of the air.

$$\text{Upward sensible heat flux} = c_p \rho \overline{wT} \quad (4.22)$$

For this estimate to be accurate, temperature and wind measurements must be taken at frequent enough intervals to define the turbulent fluctuations that produce the vertical transport. Since turbulent fluctuations are very rapid, measurements taken more frequently than every second can be required to directly measure turbulent fluxes. Inhomogeneities in surface conditions may also cause difficulty in obtaining representative fluxes from measurements taken at a single point.

By dividing the variables into a time mean and a deviation from the time mean, or eddy, we may write the upward sensible heat flux as a sum of time mean and eddy contributions.

$$w = \bar{w} + w', \quad T = \bar{T} + T' \quad (4.23)$$

Here an overbar in (4.23) indicates a time average of the quantity under the overbar and a prime indicates a deviation from that time average. Substituting (4.23) into (4.22) and performing the averages, we obtain the mean and eddy contributions to the vertical flux of temperature.

$$\overline{wT} = \overline{w}\overline{T} + \overline{w'T'} \quad (4.24)$$

Total = mean + eddy

Near the surface, the mean vertical velocity is very small compared to the typical eddy or turbulent vertical velocities, and the eddy contribution to the vertical heat flux is dominant. We can then define the latent and sensible heat fluxes as the eddy fluxes of heat and moisture at some level in the atmospheric boundary layer.

$$SH = c_p \rho \overline{w'T'} \quad LE = L \rho \overline{w'q'} \quad (4.25)$$

where ρ is air density, c_p is the specific heat of air at constant pressure, q is the specific humidity and L is the latent heat of vaporization. Measurements of the turbulent velocity, temperature, and moisture fluctuations necessary to calculate the sensible and latent energy fluxes are not routinely taken, and these rapid, small-scale fluctuations are not simulated in global climate models. In most cases, one must estimate the turbulent fluxes by using variables averaged over larger spatial and temporal scales than those of the turbulent motions in the boundary layer.

Several methods are available for estimating surface fluxes with observations of mean variables. The most common method is through the use of bulk aerodynamic formulas, which relate the turbulent fluxes to observable spatial or temporal averages. One might hypothesize that the sensible heat flux is proportional to the temperature difference between the surface and the air at some reference altitude, z_r , where mean variables are known. Since some of the kinetic energy of boundary layer turbulence comes from the mean winds blowing over the surface, we might assume that the turbulent fluxes are also proportional to the mean wind speed, U_r , at the standard height. These basic assumptions are consistent with the results of the similarity theory described previously, with which we obtain an expression that relates the sensible heat flux to the mean wind speed and temperatures.

$$SH = c_p \rho C_{DH} U_r (T_s - T_a(z_r)) \quad (4.26)$$

The latent heat flux can be related to the difference of specific humidity, q , between the surface and the atmosphere at the reference height.

$$LE = L \rho C_{DE} U_r (q_s - q_a(z_r)) \quad (4.27)$$

In the bulk aerodynamic formulas (4.26) and (4.27), ρ is the air density, c_p is the specific heat at constant pressure, L is the latent heat of vaporization and C_{DH} and C_{DE} are aerodynamic transfer coefficients for heat and moisture, respectively. Subscripts s and a indicate values for the surface and the air at the reference level, respectively.

The aerodynamic transfer coefficients depend on the surface roughness, the bulk Richardson number, and the reference height. Under ordinary circumstances, the values of the transfer coefficients for heat, moisture, and momentum would be nearly equal, and typical values for neutral stability and for a 10-m height above the surface would range from 1×10^{-3} over the ocean to 4×10^{-3} over moderately rough land. If the wind speed at 10 m is 5 m s^{-1} and $C_D = 3 \times 10^{-3}$, then from (4.26) the flux of sensible heat across the surface layer of atmosphere is about 15 W m^{-2} for each degree of temperature difference between the surface and the air at 10 m.

4.6.1 Equilibrium Bowen Ratio for Saturated Conditions

The latent heat flux depends sensitively on the temperature through the dependence of saturation vapor pressure on temperature. Over water or wetland surfaces, we may assume that the mixing ratio of water vapor at the surface is equal to the saturation mixing ratio, q^* , at the temperature of the surface.

$$q_s = q^*(T_s) \quad (4.28)$$

The vapor mixing ratio of saturated air at the reference height can be approximated with a first-order Taylor series.

$$q_a^* = q^*(T_s) + \frac{\partial q^*}{\partial T}(T_a - T_s) + \dots \quad (4.29)$$

The actual vapor-mixing ratio of the air at the reference height can be expressed in terms of the relative humidity at that level.

$$\text{RH} = \frac{q}{q^*} \quad (4.30)$$

$$q_a \cong \text{RH}(q^*(T_s) + \frac{\partial q^*}{\partial T}(T_a - T_s)) \quad (4.31)$$

Substituting (4.31) into (4.27) yields an expression for the heat loss from the surface through evaporation in terms of the temperature difference and the relative humidity,

$$\text{LE} \cong \rho L C_{DE} U_r \left(q^*(T_s)(1 - \text{RH}) + \text{RH} B_e^{-1} \frac{c_p}{L} (T_s - T_a) \right) \quad (4.32)$$

where

$$B_e^{-1} \equiv \frac{L}{c_p} \left. \frac{\partial q^*}{\partial T} \right|_{T=T_s} \quad (4.33)$$

The *Bowen ratio* is the ratio of the sensible cooling to the latent cooling of the surface. Comparing (4.32) and (4.26) we see that, when the surface is wet and the air is saturated, $\text{RH} = 1$, and assuming that $C_{DH} = C_{DE}$, the Bowen ratio takes a special value:

$$B_o \equiv \frac{SH}{LE} = B_e \quad (4.34)$$

When the surface and the air at the reference level are saturated, the Bowen ratio approaches the value B_e given by (4.33), which can be called the *equilibrium Bowen ratio*. We must assume that the flux of moisture from the boundary layer to the free atmosphere is sufficient to just balance the upward flux of moisture from the surface so that the humidity at the reference height is in equilibrium at the saturation value. The Bowen ratio in such an equilibrium is inversely proportional to the rate of change of the saturation mixing ratio of water vapor with temperature (4.33). The rate of change of the saturation-mixing ratio with temperature is very sensitive to the temperature itself. Using the approximate formula (1.9), it can be shown that

$$\frac{\partial q^*}{\partial T} \approx q^*(T) \left(\frac{L}{R_v T^2} \right) \quad (4.35)$$

The exponential dependence of the saturation-mixing ratio on temperature far outweighs the inverse square of temperature in (4.35), so that the equilibrium Bowen ratio decreases exponentially with temperature. The temperature dependencies of the saturation mixing ratio and the equilibrium Bowen ratio are shown graphically in a log-linear plot in Fig. 4.10. The equilibrium Bowen ratio is unity at about 0°C , and decreases to about 0.2 at 30°C . As the relative humidity in (4.32) is decreased from 1 to smaller values, the evaporative cooling increases, so that the equilibrium Bowen ratio is the maximum possible Bowen ratio for a wet surface. The actual Bowen ratio over a wet surface will generally be smaller than the equilibrium Bowen ratio, because the air at the reference height is usually not saturated. As a result of the strong temperature dependence of saturation vapor pressure, latent cooling of the surface dominates sensible cooling from a wet surface at temperatures

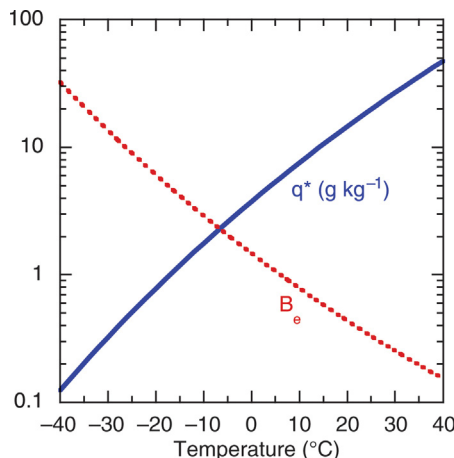


FIGURE 4.10 Saturation specific humidity $q^*(\text{g kg}^{-1})$ and equilibrium Bowen ratio B_e , as functions of temperature.

such as those in the tropics, but in high latitudes during winter sensible heat transport can be of greatest importance. To show this, assume a wet surface and saturated atmosphere, so that the actual Bowen ratio is the equilibrium Bowen ratio, we can write that

$$\frac{LE}{LE + SH} = \frac{1}{1 + B_e} \quad (4.36)$$

$B_e = 1$ at approximately 278K. At much warmer temperatures $B_e \ll 1$ and most of the surface cooling is by evaporation. At much colder temperatures $B_e \gg 1$ and most of the surface cooling is by sensible heat transfer.

The preceding discussion strictly applies only to conditions where the surface is wet, so that evaporative cooling is not constrained by lack of surface moisture. Over land areas, the evaporative cooling may be greatly reduced when moisture cannot be supplied from below the surface rapidly enough to keep the air in contact with the surface saturated. In desert areas, the surface is typically so dry that evaporative cooling is small regardless of the temperature, so that sensible cooling and longwave emission must balance solar heating. For vegetated terrain, cooling by evaporation and transpiration through leaves is controlled by the physical and biological condition of the plant canopy and the water content of the soil. The role of soil and vegetation in the surface water and energy balances is discussed further in Chapter 5.

4.7 DIURNAL VARIATION OF THE SURFACE ENERGY BALANCE

The surface energy balance is strongly influenced by the diurnal variation of insolation, except in polar regions. Figure 4.11 shows the diurnal variation of the surface radiation balance for grassland in Saskatchewan during a clear summer day with average winds. A dense mat of living and dead grass covers the surface and the surface albedo is about 16%. The average net radiation for the 24-h period shown was 155 Wm^{-2} , with 263 Wm^{-2} gained from the Sun and 108 Wm^{-2} net loss through infrared fluxes. The net downward solar radiation at the ground peaks near local solar noon at about 700 Wm^{-2} . The daytime solar heating is large because of the strong insolation, lack of cloudiness, and relatively low surface albedo. Downward longwave radiation is about 300 Wm^{-2} and does not change much during the day. The downward longwave radiation has almost no diurnal variation because of the small diurnal variation of air temperature in the free atmosphere. The surface upward emission is about 350 Wm^{-2} before sunrise and increases to about 500 Wm^{-2} at midday, in response to the warmer daytime surface temperatures. The surface temperature varies from about 10°C before sunrise to about 40°C at midday. The net longwave loss from the surface thus increases from about 50 Wm^{-2} at night to about 200 Wm^{-2} at midday. The longwave loss is relatively large because the skies are clear and the air humidity is low. The net radiation that results is an almost uniform 50 Wm^{-2} loss through longwave cooling during the night, and a strong, solar-driven gain peaking near 500 Wm^{-2} at midday.

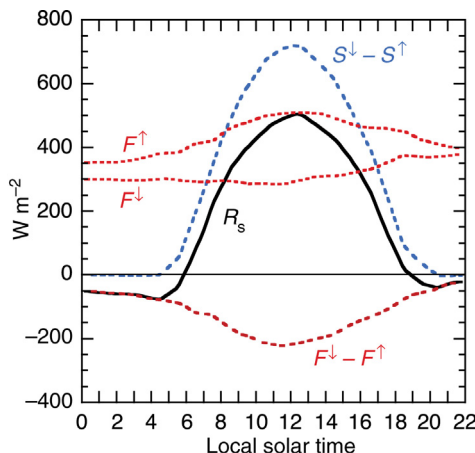


FIGURE 4.11 Components of the radiative energy balance for a grass field in Matador, Saskatchewan on July 30, 1971. F^{\downarrow} , downward longwave; F^{\uparrow} , upward longwave; $S^{\downarrow}-S^{\uparrow}$, net solar; $F^{\downarrow}-F^{\uparrow}$, net longwave; R_s , net radiation. After Ripley and Redmann (1976).

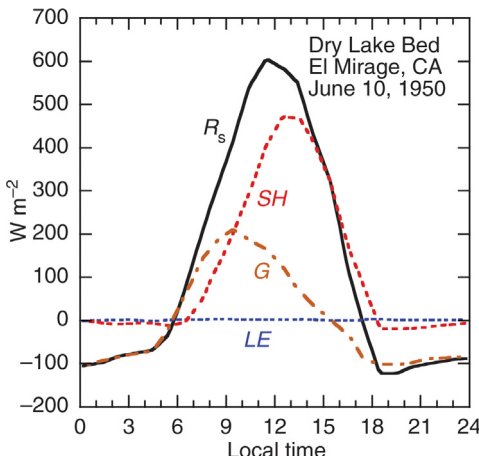


FIGURE 4.12 Heat budget for a dry lake bed at El Mirage, California on June 10, 1950. Data from Vehren camp (1953). © American Geophysical Union.

The diurnal cycle in surface energy balance components for a dry, barren lake bed is shown in Fig. 4.12. The surface soil moisture was measured at about 2% at the time the measurements were taken, so evaporation plays virtually no role in the energy balance. At night the net radiation balance is negative as the surface emits radiation into the dry desert air. The radiative cooling of the surface is balanced by energy lost from the soil as it cools through the night. Sensible heat flux is nearly zero at night because the winds are weak and the cold air near the surface is denser than the warmer air above. The high vertical stability associated with the nighttime temperature inversion suppresses the turbulent exchange of energy. Sunrise occurs at about 5 AM and the surface cooling decreases rapidly. In the early morning, the net radiative heating is largely balanced by storage of heat in the ground. After mid-morning the strong daytime radiative heating is balanced primarily by upward sensible heat flux by atmospheric turbulence. The sensible heat flux peaks shortly after noon, and by mid-afternoon the surface has begun to cool because the sensible cooling exceeds the net radiation.

The heat budget for a mature cornfield during a clear day in late summer is shown in Fig. 4.13. Again the net radiation is weakly negative at night and goes through a strong positive maximum during the day. The nighttime radiation loss is balanced about equally by release of stored surface heat, downward sensible heat flux, and dewfall. Although the corn is nearly 3 m tall, a substantial amount of heat reaches the soil so that storage in the soil and corn stalks is an important part of the energy balance during the day. The surface soil is dry, but the corn roots have sufficient water. Sensible cooling is about half of the evaporative cooling, when averaged over the day. The peculiar change in the latent and sensible cooling near noon is thought to be related to the north-south orientation of the cornrows.

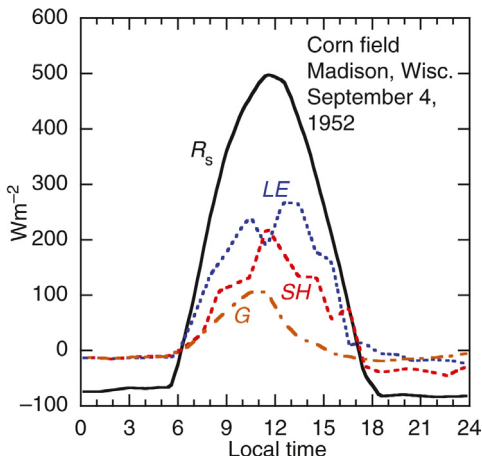


FIGURE 4.13 Heat budget for a field of mature corn in Madison, Wisconsin, on September 4, 1952. Data from Tanner (1960). Reprinted with permission from the Soil Science Society of America.

When a surface is wet, or when growing vegetation has ample soil water for evapotranspiration, the net radiation may be almost entirely used for evaporation, with the soil storage and sensible heat fluxes being of minor importance. When warm and dry air moves over a surface with ample water, the evaporative cooling may actually exceed the net radiation. Figure 4.14 shows the energy balance on a day when winds carry

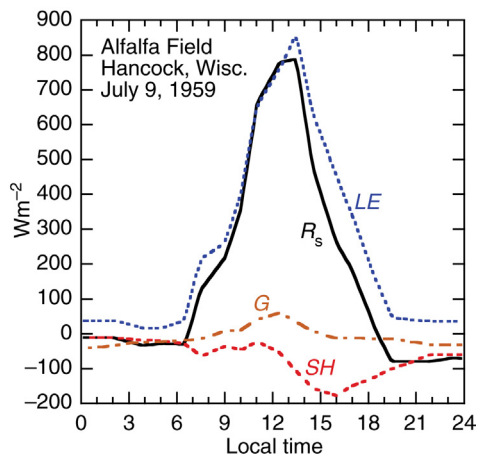


FIGURE 4.14 Heat budget for a well-irrigated alfalfa field in Hancock, Wisconsin on July 9, 1956, when the air was advected to the field from a warm dry area. Data from Tanner (1960). Reprinted with permission from the Soil Science Society of America.

warm dry air over a well-irrigated alfalfa field. Evapotranspiration equals or exceeds the net radiation at every hour of the day, and evaporation continues even through the night. The excess of the evaporative cooling over the net radiation is provided by downward sensible heat flux, with turbulent motions carrying heat downward to the evaporatively cooled surface. For small, irrigated plots in hot, arid regions, the sensible heating of evaporatively cooled surfaces can add to the water demand.

4.8 SEASONAL VARIATION OF THE ENERGY BALANCE OF LAND AREAS

The energy balance of the surface changes with season, especially in middle and high latitudes, where large seasonal variations of insolation and temperature occur. In tropical regions, the energy balance may change because of seasonal changes in precipitation, even when the temperature and insolation remain relatively constant. The seasonal variation of the components of the surface energy balance at several locations in middle latitudes is shown in Fig. 4.15. The annual variation of net radiation generally follows that of insolation, with peak values in summer approaching 200 Wm^{-2} in land areas, depending on the latitude, sky conditions, and surface albedo. Water surfaces in relatively cloudless areas can have summertime net radiation near 300 Wm^{-2} . The mechanism for balancing this net radiation depends on the local surface conditions. Over land areas, it is primarily a question of whether the mechanism is latent or sensible cooling, since storage is small and transport is zero. The apportionment between sensible and latent cooling depends on the availability of surface moisture, the temperature, and the humidity of the air.

In regions with significant precipitation during the summer season, where the surface remains relatively moist, the latent cooling is generally limited by and follows the annual cycle of radiative heating. Where the climate is exceptionally dry, such as in Yuma, Arizona, the latent cooling is negligible, except during months with precipitation. At Yuma, significant evaporation occurs in the springtime and during September. Flagstaff, Arizona, is at a higher elevation than Yuma and the mountains receive significant summertime precipitation. As a result, the evaporative cooling during summer is greater than at Yuma.

At West Palm Beach, Florida, the winters are relatively dry, so that the springtime insolation increase is initially balanced by equal contributions from latent and sensible cooling of the surface. As the summertime convective precipitation begins to wet the surface, the evaporative cooling takes over. At San Antonio, Texas, the surface dries out during spring and summer, so that a gradual increase in the importance of sensible heating occurs over the course of the summer months. At Astoria, Oregon, sensible

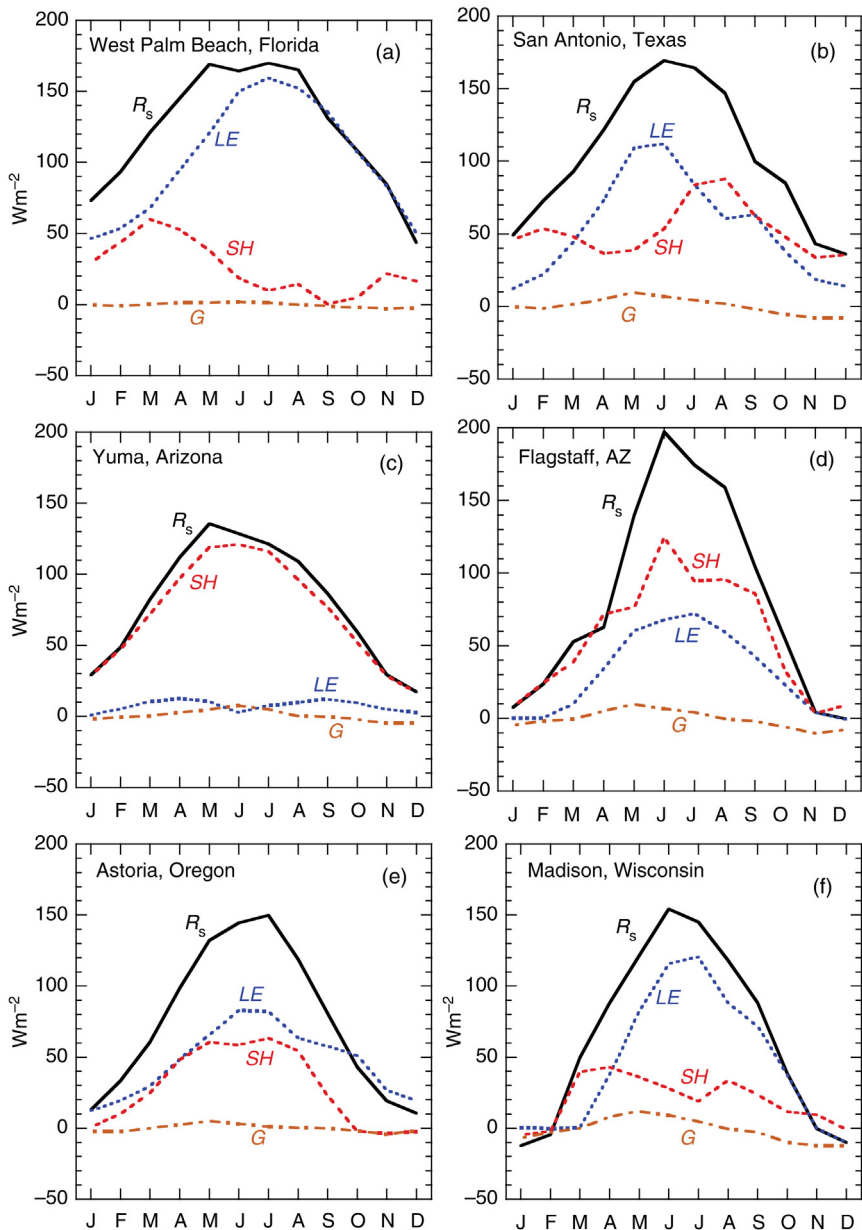


FIGURE 4.15 Annual cycle of heat budget components for various mid-latitude land locations. Adapted from Sellers (1965). Reprinted with permission from the University of Chicago Press.

cooling is important in the summer, even though Astoria gets more annual precipitation than Madison, Wisconsin, where evaporative cooling dominates during summer. This is because the precipitation at Astoria peaks in the winter, when little energy is available for evaporation, so that about 70% of the annual precipitation runs off before being evaporated. During the summer, relatively little precipitation falls at Astoria. At Madison, precipitation peaks in the summer when the large net radiation provides the energy to evaporate large amounts of water that later is released in convective weather systems such as thunderstorms.

In ocean areas, the heat capacity of the water is sufficient that the energy for evaporation may be derived from the energy of the water itself. The evaporative loss may be less correlated with net radiation than with factors such as the wind speed or the temperature and humidity contrast between the surface and the air above it. Much of the high-latitude evaporation over the oceans takes place in winter over the Kuroshio and Gulf Stream currents. These currents carry warm water poleward along the western margins on the Pacific and Atlantic oceans where it comes into contact with cold, dry air coming off the continents. The combination produces evaporation rates near 400 W m^{-2} in these regions during winter. Figure 4.16 shows estimates of the annual cycle of surface energy fluxes over the Gulf Stream at 38°N . The annual variations in most terms are much larger than that of the net radiation. Enormous latent cooling rates in winter are balanced primarily by the release of energy stored in the water temperature and import of heat through horizontal transport.

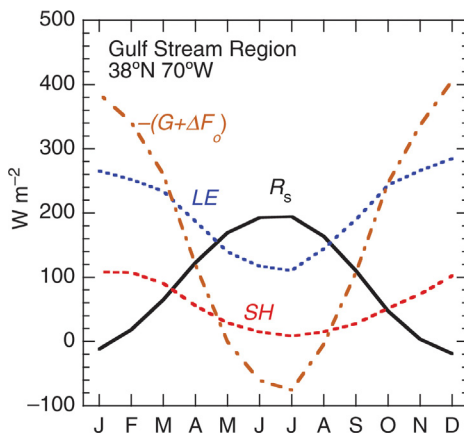


FIGURE 4.16 Annual cycle of the surface heat budget components for the region near 38°N , 70°W , which is affected by the Gulf Stream. Note that storage plus export has been plotted with reversed sign; heat converges and is lost to the atmosphere in winter. Data from ERA-Interim Reanalysis.

4.9 GEOGRAPHIC VARIATION OF THE SURFACE ENERGY BALANCE

Some intuition about the relative importance of the various components of the surface energy budget as a function of the climatic regime can be gained from their dependence on latitude. The net radiation at the surface peaks in the tropics, following the general pattern of insolation at the top of the atmosphere (Fig. 4.17). The upward and downward longwave fluxes are much larger than the net solar, but the downward longwave irradiance is almost as large as the upward irradiance, so that longwave radiation produces a weak cooling of the surface. The latent cooling term mirrors the insolation fairly closely (Fig. 4.18), since globally most of the radiative heating of the surface is used to evaporate water. The sensible cooling of the surface is much smaller and more uniform, with a slight increase over the Northern Hemisphere where more land is present. The ocean transports heat from near the equator toward the extratropics, but its influence is smaller than the other terms that represent the vertical movement of energy.

The geographic variation of the annual mean surface heat balance components are shown in Fig. 4.19. Net radiation is greatest over the tropical oceans, where the surface albedo is low and the surface temperature is moderate. In these regions, it often exceeds 180 W m^{-2} . Most of the variation in net radiation comes from the latitudinal decrease of insolation and from cloudiness variations and their effect on surface solar heating. In high latitudes, the annual mean net radiative heating of the surface approaches zero.

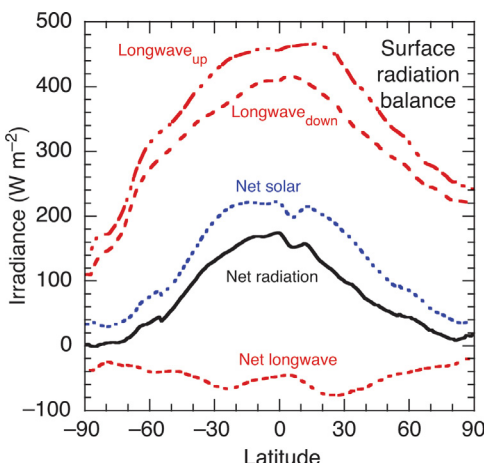


FIGURE 4.17 Components of the annual average surface radiation budget plotted against latitude. Data from Lin et al., 2008.

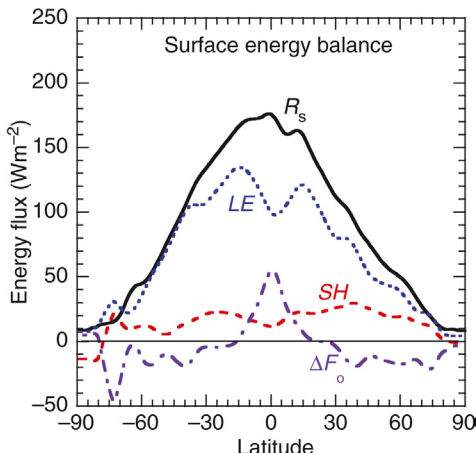


FIGURE 4.18 Components of the annual average surface energy balance plotted against latitude. Data smoothed and adjusted from Lin et al., 2008.

The evaporative heat loss from the surface has its greatest values over the mid-latitude, warm, western boundary currents, the Kuroshio and the Gulf Stream (Fig. 4.19b). In these regions at the western edges of the Pacific and Atlantic oceans, the evaporative heat loss may exceed 200 Wm^{-2} and is much greater than the local net radiative heating of the ocean surface. The evaporative cooling of the western boundary currents is greatest in the winter season. However, these areas are relatively small. The evaporative heat loss is also large over the expanses of the subtropical oceans, where evaporation consumes most of the energy provided to the surface by net radiation. Evaporation driven by insolation over the tropical and subtropical oceans is the boiler that drives the circulation of the atmosphere and the hydrologic cycle of Earth.

The sensible heat loss is largest from relatively dry land areas. The sensible heat loss from the ocean surface is small, except over the warm western boundary currents of the mid-latitude oceans (Fig. 4.19c). These large sensible heat fluxes occur when cold air from the continents flows over the warm ocean currents during winter. In these regions, sensible heat fluxes may exceed 50 Wm^{-2} in the annual mean, but they are still much less important than evaporative cooling.

The divergence of the heat flux in the ocean, or alternatively, the flux of heat from the atmosphere into the ocean, is large and negative over the western boundary currents (Fig. 4.19d). In these regions, the ocean is supplying heat by horizontal transport in the oceans, which is then lost to the atmosphere. The regions where the air is heating the water are found

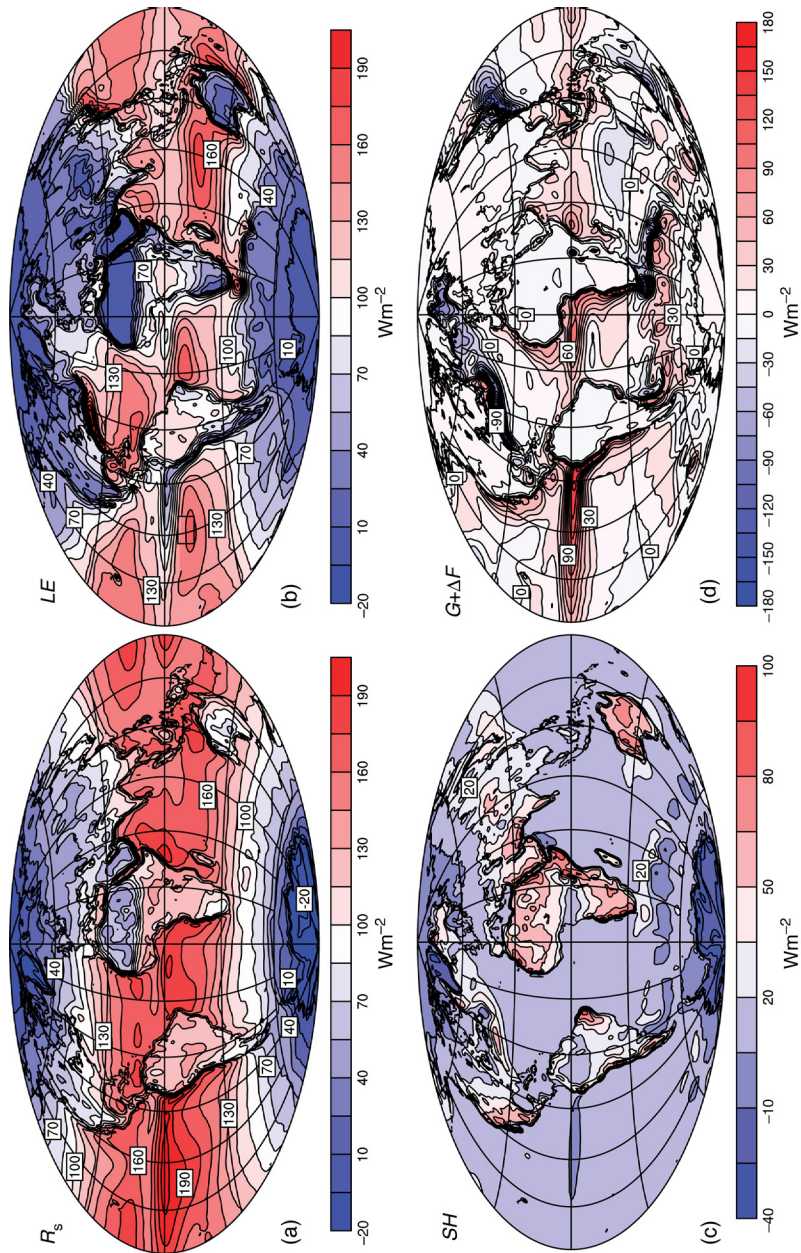


FIGURE 4.19 Global maps of the annual average surface energy budget components. (a) Net surface radiation; (b) latent heat flux; (c) sensible heat flux; (d) net downward heat flux into the ocean. Based on ECMWF ERA-interim reanalysis data products.

along the equator and along the eastern margins of the oceans where upwelling brings cold water to the surface. In these regions of upwelling, latent heat loss is reduced and more of the net radiation is used to heat the ocean water. The large transfers of energy from the tropical and eastern oceans to the mid-latitude western oceans in the Northern Hemisphere play a critical role in determining the climate of maritime areas. The ocean currents that produce these important energy transports are described in Chapter 7.

EXERCISES

- If the top 100 m of ocean warms by 5°C during a 3-month summer period, what is the average rate of net energy flow into the ocean during this period in units of Wm^{-2} ? If the atmosphere warms by 20°C during the same period, what is the average rate of net energy flow into the atmosphere?
- In (4.4) the heat content of the atmosphere is estimated as $c_p T(p_s / g)$, but in a compressible, hydrostatic atmosphere the potential energy of the atmosphere, gz , must also increase when it warms, since the atmosphere is raised as it warms. Use the hydrostatic relationship to estimate how much the required increase in potential energy adds to the heat capacity of the atmosphere, if the atmosphere warms by the same amount at all pressures.
- Derive (4.18) from (4.15) and (4.17).
- The blackbody emission from the surface can be linearized about some reference temperature T_0 . $\sigma T_s^4 \approx \sigma T_0^4 + 4\sigma T_0^3(T_s - T_0) + \dots$. And the sensible cooling of the surface can be written as $\text{SH} \approx c_p \rho C_D U(T_s - T_a) + \dots$. Calculate and compare the rates at which longwave emission and sensible heat flux vary with surface temperature, T_s . In other words, if the surface temperature rises by 1°C, by how much will the longwave and sensible cooling increase? Assume that $T_0 = 288 \text{ K}$, T_a is fixed, $\rho = 1.2 \text{ kg m}^{-3}$, $c_p = 1004 \text{ J kg}^{-1} \text{ K}^{-1}$, $C_D = 2 \times 10^{-3}$, and $U = 5 \text{ m s}^{-1}$.
- Air with a temperature of 27°C moves across a dry parking lot at a speed of 5 m s⁻¹. The insolation at the surface is 600 Wm⁻² and the downward longwave radiation at the ground is 300 Wm⁻². The longwave emissivity of the surface is 0.85, and the albedo of the asphalt surface is 0.10. What is the surface temperature in equilibrium? What is the surface temperature if the asphalt is replaced with concrete with an albedo of 0.3 and the same emissivity? The air density and drag coefficient are as in problem 3. Hint: Linearize the blackbody emission around the air temperature and use the surface energy equation to show that, $T_s - T_a = \frac{S^\downarrow(0)(1-\alpha_s) + \varepsilon(F^\downarrow(0) - \sigma T_a^4)}{c_p \rho C_D U + \varepsilon 4\sigma T_a^3}$.

6. Do problem 4 for the case in which the parking lot is wet and the air is maintained just at saturation, and include the effect of latent cooling of the surface. Ignore any effects of surface water on the albedo. Compare the surface temperature for wet and dry surfaces. How would the results differ if the air was not saturated? *Hint:* Make use of (4.34).
 7. Give the reasons why the net radiation at the surface at Flagstaff is greater than the net radiation at Yuma during summer ([Fig. 4.15c,d](#)).
-